High-Throughput Discovery of Structure−Mechanical Property Relationships for Segmented Poly(urethane−urea)s

Joe-Lahai Sormana and J. Carson Meredith*

School of Chemical and Biomolecular Engineering, Georgia Institute of Technology, Atlanta, Georgia 30032-0100

Received September 16, 2003; Revised Manuscript Received January 19, 2004

ABSTRACT: A novel high-throughput method was used to determine the effect of chain extender composition on the mechanical properties of segmented poly(urethane−urea)s. Combinatorial libraries with continuous gradients in chain extender composition ($60 < \phi < 160$ mol % stoichiometry), cure temperature ($70 < T < 110$ °C), or both were synthesized. Stress vs strain data were obtained at numerous library positions (corresponding to different ϕ values) using a unique high-throughput mechanical characterization (HTMECH) apparatus developed by the authors. These mechanical measurements were related to the morphology, hydrogen bonding, and degree of phase separation using AFM, FTIR, and DSC. Optimum strength and percent elongation were observed at a chain extender composition of $\phi =$ 85 mol %, corresponding also with the finest phase-separated morphology, indicated by an even dispersion of uniform hard domains (dimensions 110−130 nm). DSC measurements indicated increased mixing of soft and hard segments when ϕ exceeded 85%, which was correlated to decreased urea−urea hydrogen bonding (from FTIR). SEM analysis of the library fracture surfaces suggested a transition from brittle to ductile failure with increased ϕ, in agreement with the increased soft−hard segment mixing and disruption of the hydrogen-bonded network. These results validate the HTMECH approach as an accurate and effective screening tool for developing mechanical property−structure relationships in combinatorial polymer libraries.

Introduction

The successful application of combinatorial and high-throughput methods (CHM) in the pharmaceutical industry has made these techniques very attractive to materials researchers. Compared to conventional one-sample−one-measurement techniques, CHM provides a cost- and time-saving alternative, especially during the discovery stages of a materials research endeavor. In polymer materials research, the purpose of CHM is not to replace established measurement techniques, but rather to enhance the use of detailed measurement techniques by providing an efficient screening to select the most relevant regimes of parameter space to explore. This is accomplished by exploring a large variable space with high-throughput screens of desired properties on a single library, reducing variance and the likelihood of overlooking unexpected behavior.

To apply CHM to polymer research, methods have been developed for preparing high-throughput polymer libraries with continuous gradients in composition, thickness, surface energy, and annealing temperature (T).[1−5] These libraries have been used to characterize polymer blend phase separation,[1] thin-film dewetting,[2,6] block copolymer surface pattern formation,[7] crystallization growth rate,[5] cell adhesion and function on polymer surfaces,[8] and mechanical properties of polymer films.[9−11] In addition, discrete sample libraries that explore variations in composition and chemical structure have been developed.[12−14] With numerous library preparation techniques available (gradient and discrete), the limitation in polymer CHM appears to be in the screening and characterization stage. There is a strong need to extend the suite of high-throughput screens available for polymers. For example, polymeric materials are especially sensitive to processing variables such as temperature and rheological history, which strongly affect the nano- and microstructures. These microstructures have a tremendous effect on mechanical, thermal, optical, and permeability properties. Polyurethanes and poly(urethane−urea)s are good examples of this sensitive relationship between processing, structure, and mechanical properties.

Segmented poly(urethane−urea)s are elastomers that belong to the group of materials generally referred to as "polyurethanes". Compared to traditional polyurethanes, segmented poly(urethane−urea)s have superior elasticity and strength[15] due to improved phase segregation and a three-dimensional bidentate urea−urea hydrogen-bonding network found in the hard domain.[16,17] Because of the myriad block chemistries and microstructures possible, SPUU elastomers have a wide range of applications, including biomaterials, textiles, foams, coatings, adhesives, and other consumer products. Despite the industrial importance of SPUUs, there is still limited literature addressing the effect of chain extender stoichiometry on mechanical properties of poly(urethane−urea)s,[18] in particular in combination with varying the cure T. One problem is the large number of combinations of soft and hard segment chemistry, isocyanate chemistry, chain extender composition, and cure T values. Large numbers of combinations are difficult to screen with conventional sample preparation techniques, particularly given the sensitivity of isocyanates to water contamination and small errors in the mixing of compositions.

To understand this complexity, consider that the mechanical properties of SPUUs are dependent on the degree of phase separation between hard and soft segments. Generally, a finer morphology results in higher elongation at break and tensile strength.[16] The

* Corresponding author: Tel 404-385-2151; Fax 404-894-4200; e-mail Carson.Meredith@chbe.gatech.edu.

10.1021/ma035385v CCC: $27.50
Published on Web 02/25/2004

degree of phase separation in polyurethanes is dependent primarily on cure temperature and chain extender composition and has been monitored using FTIR, DSC, X-ray diffraction, and AFM.[15−17,19−26] Although the literature is limited for SPUUs, extensive investigation of polyurethanes has shown that the morphology and mechanical properties are affected strongly by the molar ratio of isocyanate to chain extender,[27−36] insight which is expected to apply to SPUUs as well.[37] Changing the ratio of isocyanate to chain extender can alter the amount of hydrogen bonding by causing a relative excess or depletion of N−H hydrogen donors.[18] A stoichiometric excess of isocyanate or the use of tri- or higher functional chain extenders can lead to biuret (urea groups) and allophanate (urethane groups) chemical cross-links.

To address the need for high-throughput screens capable of determining such processing−structure−mechanical property relationships, we reported previously a new apparatus for high-throughput mechanical characterization (HTMECH) of polymer libraries.[9] We applied HTMECH to characterize structure−property relationships in poly(urethane−urea) *T*-gradient libraries.[10] In the present paper, we use HTMECH to develop structure−property relationships for segmented poly(urethane−urea) (SPUU) libraries with a gradient in chain extender composition (ϕ). There are several key questions we seek to answer in this study. First, we desire to demonstrate that the combinatorial library synthesis technique mentioned above can be used to synthesize polymers (in this case a block copolymer) in situ on ϕ-gradient libraries. Previously, these libraries were used only to blend polymers and other additives. Below, we describe the preparation of ϕ-gradient combinatorial SPUU library films, which are subsequently annealed over an orthogonal *T*-gradient to examine the combined effects of varying both the curing *T* and chain extender composition. The libraries are characterized (screened) with high-throughput spectroscopic, microscopic, and mechanical measurements at points representing different chain extender ϕ and cure *T*. Second, we seek to discover whether relatively simple spectroscopic screens, e.g., FTIR, can be used to indicate structures that predict optimal mechanical properties. Stress−strain profiles are related to the materials microstructure using FTIR, AFM, and DSC, and we show that the urea−urea H-bonding fraction determined from FTIR is a good predictor of trends observed with tensile strength. Finally, we will present a rigorous comparison between HTMECH and conventional uniaxial tensile tests to determine the reliability of HTMECH relative to existing methods for mechanical measurements.

Experimental Section

Materials and Library Synthesis. Segmented poly(urethane−urea) libraries were synthesized by first preparing two solutions: (1) toluene diisocyanate (tetramethylene glycol) prepolymer (Air Products and Chemicals, AIRTHANE PET-85A, M_w = 2500, NCO functionality = 2.0, mass % NCO = 3.3%) and (2) trimethylene glycol di-*p*-aminobenzene chain extender (Air Products and Chemicals, VERSALINK 740-M), to a total concentration of 30 mass % in tetrahydrofuran (VWR, ACS Grade). A composition-gradient film library was prepared by using a technique described in detail elsewhere.[1,38,39] A clean vial was initially loaded with 1 cm^3 of the prepolymer and chain extender solutions mixed at 60 mol % of the stoichiometric amount of chain extender. The solution was stirred vigorously, and the infusion pump, the withdrawal pump, and the automated sample syringe were activated simultaneously to (1) infuse 0.20 cm^3 of the 30% by mass chain extender solution into the vial at 0.14 cm^3/min, (2) withdraw 0.40 cm^3 of the solution from the vial at 0.30 cm^3/min, and (3) extract continuously the mixed solution in the vial. After a sampling period of 40 s, the sampling syringe contained 70 μL of solution with a linear gradient in chain extender stoichiometric amount (60−157 mol %) along the length of the syringe needle. Although gradient library films were prepared from 60 to 157 mol % curative, the characterization was performed over a narrower range, 80−150%, to avoid the edges that might contain residual stresses or other artifacts. The content of the syringe needle was deposited as a 25 mm long stripe on a silicon wafer (Silicon Inc.) within 16 s. The gradient stripe was placed quickly under a 40 mm wide stationary knife edge (350 μm above the substrate at a 5° angle) and was coated quickly as a film for a distance of 30 mm by moving the substrate under the blade at 25 mm/s, orthogonal to the composition-gradient direction. Multiple composition-gradient films were prepared in the same manner with thicknesses between 20 and 35 μm. The library was cured by placing a composition-gradient film on a linear temperature-gradient stage,[1,38,39] under −1 atm vacuum, for 6 h. The lower and upper end point temperatures of the heating stage were set to 75 and 110 °C, respectively. Some of the composition-gradient libraries were cured at a uniform temperature (90 °C) in a vacuum oven for 6 h.

Characterization. a. Spectroscopy. The thickness at different positions on the films, corresponding to different combinations of chain extender stoichiometry and cure temperature, was measured by visible−near-infrared interferometry (Stellar Net EPP 2000). Interferograms collected from wavelengths of 400−900 nm were fitted numerically to a thin film optics model using Film Wizard software (SCI). Refractive index and optical adsorption were measured as a function of wavelength with variable-angle spectroscopic ellipsometry (V-VASE, J.A. Woollam Co). FT-IR absorption spectra were recorded at room temperature and a resolution of 4 cm^{-1} using a Bruker IRscope II connected to a Bruker IFS 66/V spectrometer. The IR microscope was equipped with an *x*−*y* translation stage which facilitates rapid screening of the polymer libraries. The sample area was purged with dry air to prevent the appearance of atmospheric water bands in the spectra. The poly(urethane−urea) films were mounted on a sapphire substrate, and spectra were recorded at different positions on the gradient film libraries. The spectra were corrected for thickness differences, and a peak separation and analysis software package (Peakfit 4.11, Jandel Scientific) was used to resolve the bands in the carbonyl region (ν = 1630−1740 cm^{-1}) to obtain the relative ratios of the peak areas, assuming Gaussian peak shapes.

b. Microscopy. AFM images of the films were taken in the noncontact (tapping) mode at different positions using a Thermomicroscopes SPM Explorer. An *x*−*y* translation stage was attached to the microscope, which allows relatively high-throughput screening of different library positions. The images were acquired under ambient conditions with SFM (Thermomicroscopes # 1650) silicon probes, having a resonant frequency of 292−331 Hz and a spring constant of 24−41 N/m. The length, width, and thickness of the probe are 126, 27−28, and 10−15 μm, respectively. The set point amplitude used in feedback control was adjusted to 50−70% of the tip's free amplitude of oscillation. The AFM was operated on a vibration isolation table.

c. Mechanical Tests. Libraries were deformed at various *T*, ϕ positions using the HTMECH apparatus, shown schematically in Figure 1. Details on the development of this apparatus can be found elsewhere.[9,10] These previous papers also discuss experiments that illustrate the excellent reproducibility of force vs deformation data and mechanical parameters extracted from these data. Generally there is less than a 5% variability in forces between various points measured on a uniform composition library. Also, no artificial correlations have been observed for neighboring measurements on the library. Stress vs strain profiles were obtained at two strain

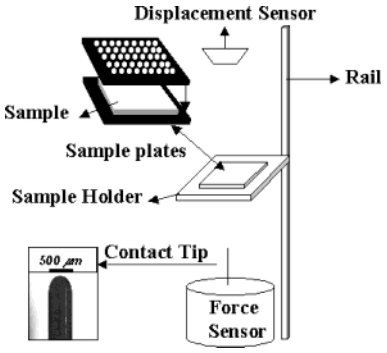

Figure 1. Schematic representation of the high-throughput mechanical characterization apparatus.

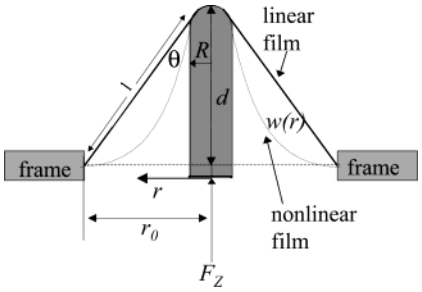

Figure 2. Schematic representation of film deformation geometry.

rates: an impact rate of 0.9 m/s and a slow rate of 30 mm/min (0.5 mm/s). All mechanical tests were performed under ambient conditions. After indentation, the films were coated with a thin layer of gold, and SEM images of the fracture surfaces were taken using a Hitachi 3500H SEM. To compare mechanical measurements from HTMECH (radial geometry) to the conventional uniaxial tensile tests, five samples of uniform chain extender composition of 85, 100, 116, 132, and 150 mol % were cured in a vacuum oven at 90 °C for 6 h. These samples were characterized mechanically using both the HTMECH apparatus and a commercial uniaxial tensile apparatus (Instron 5842) at a strain rate of 30 mm/min. DSC measurements of these uniform samples were carried out on a Seiko DSC220C differential scanning calorimeter over the temperature range of −90 to 90 °C at a heating rate of 5 °C/min. The degree of chemical cross-linking was estimated by placing 30−50 mg in a glass vial containing 5 cm^3 of *N*,*N*-dimethylformamide (DMF) for a week, followed by gravimetric determination of the nonsoluble fraction.

Figure 2 shows a cross section of the deformation geometry in the HTMECH apparatus. The load on the needle, e.g., the force that is measured, F_Z, is the vertical component of the actual in-plane radial tensile force (F_r) developed in the film. In Figure 2, the film profile is represented in two ways: (1) the actual profile that can have some degree of nonlinearity and (2) a linear approximation or conical film profile shape. The geometrical parameters include d, the indentation distance; r, the radial position measured from the center of the needle; $w(r)$, the film profile shape; R, the needle radius (R = 500 μm); l, the extended length of the film in the linear approximation; r_0, the hole radius (r_0 = 3 mm); and θ, the tangent angle between the film and the needle at their point of contact, $r = c$.

Green and Adkins[40] presented the general theory of large deformations of elastic membranes: thin materials that do not exhibit bending stresses (normal to plane of material) under a load. Thin elastomeric polymers are thought to come close to the ideal membrane model, where all of the stress is distributed in the plane of the material, with both radial and tangential components, $\sigma_r(r)$ and $\sigma_t(r)$. The deformation of axisymmetric membranes (Figure 2) is treated by Yang and Feng,[42] who presented a numerical solution of the geometry employed in this work, namely a circular membrane deformed by a spherical tip, shown recently to correlate well with experimental measurements.[44] It is important to emphasize that experimental conditions only approximate equilibrium in the case of slow strain rates, whereas large strain rates are likely to be far from equilibrium. Nevertheless, an examination of membrane theory sheds important physical insights onto the HTMECH apparatus design and interpretation of results.

To understand the measurement geometry employed in this work, it is desirable to know how the film profile, $w(r)$, and stresses, $\sigma_r(r)$ and $\sigma_t(r)$, depend on the load, F_Z, sample geometry, and material properties. In the absence of significant flexural rigidity, eqs 1 and 2 describe the relationship between these parameters and must generally be solved numerically or through infinite series.

$$\sigma_r \frac{dw}{dr} = \frac{rF_Z}{2} \tag{1}$$

$$\frac{d}{dr}(\nabla^2 f) + \frac{Eh}{2r}\left(\frac{dw}{dr}\right)^2 = 0 \tag{2}$$

In the expressions above, $f(r)$ is the stress function, from which $\sigma_r = (1/r)(df/dr)$ and $\sigma_t = d^2f/dr^2$. Wan and Liao[43] presented an analytical solution in two limiting cases that are particularly relevant to the geometry employed here. The film profile is divided into a contact region (where tip contacts film) and a noncontact region (extending from contact radius, $r = c$, to the mounting edge, $r = r_0$). In the contact region, the solution is simplified because the film profile is constrained to follow the tip shape. To obtain an analytical solution in the noncontact region, the authors adopted two different assumptions about the film profile and stress distribution. In the conical approximation, it is assumed that the film profile is a simple linear function (see Figure 2). In the uniform stress assumption, the stress is assumed to be distributed uniformly throughout the noncontact region, e.g., $f \neq f(r)$. It turns out that these two solutions offer approximate maximum and minimum bounds on what is observed experimentally. In addition, their solutions predict the dependence of load, F_Z, vs indentation, d, on the ratio of the tip radius to the hole radius, R/r_0. Of particular interest is that both approximations predict that as $R/r_0 \rightarrow 0$ (the point-load limit) the load scales with indentation as, $F_Z \sim d^n = d^3$, which is a common characteristic of thin films.[43] As $R/r_0 \rightarrow 1$, n becomes larger than 3.

The models above assume purely elastic materials with no bending (z-component of film stress). In reality, one wishes to understand how the onset of plastic deformation or presence of bending might affect the load−indentation data. The experiments of Wan and Liao[43] indicate that when plastic yielding does occur, it begins at the contact point between tip and film, $r = c$, and decreases as $r \rightarrow r_0$, with a maximum at c. The conical profile assumption (nonconstant stress function) predicts a minimum tip radius to prevent yielding $R \geq 9F_Z/(2\pi h\sigma_y)$, where σ_y is the yield stress. Thus, for a constant yield strength, the onset of plastic deformation will be enhanced by smaller tip radius, larger loads, and thinner films. To avoid plastic yielding, which is not a design necessity of ours, the yield stress must stay above $\sigma_y = 95F_Z$ (MPa), corresponding to a maximum σ_y of 430 MPa at our highest observed loads. SPUUs generally stay outside of this σ_y range due to their highly elastomeric nature. However, deviations from elastomeric behavior are observed for some library compositions in which the elastomeric network is compromised. In these cases, plastic yielding can occur if σ_y becomes significantly small, which actually is a convenient indicator of elastomer network quality. In addition, Wan and Liao's experiments discuss the influence of tip radius on the stretching vs bending behavior of real films that have a nonzero bending component. There is a corresponding maximum tip radius, R, for the film to undergo pure stretching. Our apparatus has $R/r_0 = 0.25/1.5 = 1/6$, and to avoid bending stresses, our tip radius, $R = 0.5$ mm, is always well below the predicted maximum $R = 400F_Z$ (mm), where F_Z is the load in N. To calculate this parameter,

we estimate the flexural rigidity of common poly(urethane−urea)s as $D = E_Y h^3/12(1 - \nu^2) \approx 10^{-8}$ J, where E_Y (elastic modulus at 100% strain) ≈ 3 MPa and ν (Poisson's ratio) = 0.5.[43] For films that have significant flexural rigidity, or large thickness, the gradient of F_Z vs d is predicted to fall below $n = 3$, with $n = 1$ at pure bending.

A primary objective of this work is to compare results for mechanical measurements from both uniaxial and biaxial instruments, rather than to make detailed comparisons to theory. Hence, we choose operational definitions of stress and strain that allow a meaningful comparison to the uniaxial data. The raw force vs time data were converted to an "operational" stress (σ) by dividing force by the area around the hole perimeter where the film is held: area $= 2\pi r_0 h$, where h is the initial film thickness. For simplicity, we assume a linear profile and note that in most cases the film profile conformed closely to a conical geometry. The engineering strain (ϵ) was obtained by dividing the instantaneous linear radial deformation, $l = l(t)$, by the initial hole radius, r_0. The radial deformation was obtained by first converting time (t) into vertical needle indentation, $d = v_0 t$, where the strain rate v_0 changes by less than 1% during impact.[9,10] The linear deformation is found as the hypotenuse between the fixed hole radius, r_0, and d: $l = (d^2 + r_0^2)^{1/2}$.[10] The radial component of the force is obtained from trigonometry as $F_R = F_Z/\cos(\theta)$, where $\cos(\theta) = d/(d^2 + r_0^2)^{1/2}$ (Figure 2). Measurement of the radial force from the measured vertical force can lead to problems at low elongation, where the needle becomes nearly perpendicular to the film and $\cos(\theta) \approx 0$, but this is confined to the first 10−20% of strain. In addition, when the actual film profile deviates significantly from linear, the true θ value will be less than the linear approximation, leading to an overestimation of σ and underestimation of ϵ. Fortunately, these errors will cancel in the calculation of an "effective" secant modulus: $E = d\sigma/d\epsilon = [F_Z(d^2 + r_0^2)^{1/2}/(2d\pi r_0 h)]/[(d^2 + r_0^2)^{1/2}/r_0] = [F_Z/2\pi dh]$. The $[(d^2 + r_0^2)^{1/2}]$ term indicating the instantaneous deformed film radius cancels, and this operational modulus should be identical from both uniaxial and biaxial tests, barring any other artifacts. We note that the secant modulus is not Young's modulus.

Differences in mechanical response in uniaxial vs radial strain may occur due to geometry-dependent stress nonlinearity and nonaffine deformation in elastomer networks. Radial deformation is a special case (the equibiaxial strain case) of the more general biaxial deformation. Recent studies on cross-linked and entangled PDMS elastomers show that biaxial deformations are more sensitive to these nonlinear and nonaffine effects than uniaxial strains.[45] First of all, it is well-known that affine elastomer deformations exhibit significant nonlinear stress vs strain profiles, even when single chains are assumed to be linearly elastic (Gaussian).[46] In an affine deformation, network connection sites are displaced homogeneously in proportion to the bulk sample dimensions. At moderate strains, network connectivity allows heterogeneous rearrangements that can reduce the stored stress below what would be predicted for an affine deformation. As a result, elastomers show nonaffine deformations whose magnitude is dependent on the loading geometry. We can expect differences in the modulus between the uniaxial (one loaded dimension) and radial (two loaded dimensions) test geometries to arise due to the nonlinear stress response and the nonaffine deformations. In addition, the strain-induced crystallization common for SPUU elastomers (usually at strains exceeding ≈300%) is also dependent on the strain geometry. These predictions will be examined below in a comparison of results from the radial HTMECH apparatus vs conventional uniaxial deformation.

One may also be concerned with the effect of the composition gradient on the measured properties. We have compared gradient library results to results from uniform films for the compositions explored here and have found no significant deviations in the trends observed. To our knowledge, no theory has been developed that predicts the effect of a gradient in modulus, for example, on the deformation. Such a development would be beyond the scope of the present paper. In other high-throughput measurements, e.g., microscopy, it was noted that the steepness of the gradient plays a critical role in determining whether the gradient artificially influences results.[7] Intuition leads one to suspect that an asymmetrical film profile would result, and the force on one side of the needle would be less than the other. If the gradient were significantly steep, this could lead to bending of the needle, an artifact that was not observed in our experiments.

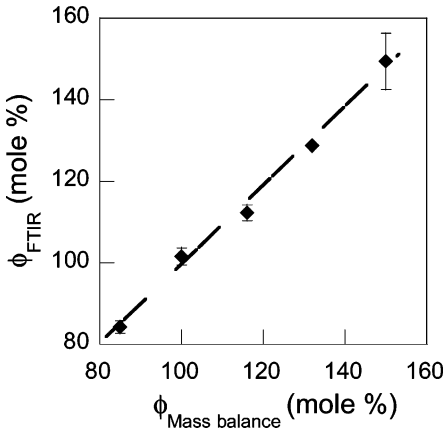

Figure 3. Verification of chain extender composition in gradient library using FTIR.

Results and Discussion

The chain extender composition at different positions on the composition-gradient library was calculated using the mass balance equation developed elsewhere.[1] These predicted compositions (based upon coating conditions) agree very well with data obtained from FTIR (see Figure 3) using a calibration curve (not shown) of known chain extender compositions based upon the absorption area of two carbonyl peaks centered around 1707 and 1730 cm^{-1}. This check indicates the degree of control over composition that is typical of the ϕ-gradient coating procedure.

Twenty-five FTIR spectra were taken from a 2D T,ϕ-gradient library, corresponding to different combinations of cure T and chain extender composition ϕ. The fraction of total urethane, urea−urea, and total urea hydrogen bonding was estimated using appropriate ratios of H-bonded and free carbonyl peaks, as reported by others.[24] Particularly important in determining mechanical properties is the bidentate urea−urea hydrogen bonding, which is believed to form a three-dimensional network that improves hard and soft phase segregation relative to nonurea polyurethanes.[16,17]

Figure 4 shows FTIR spectra in the N−H stretch region taken at different ϕ positions on a ϕ-gradient library cured at 90 °C. The two peaks in the spectra are identified as free N−H (ν = 3363 cm^{-1}) and hydrogen-bonded N−H (ν = 3292 cm^{-1}). There is a relative increase in the free N−H absorption with increasing ϕ, shown by a calculation of the peak areas. This relative increase in free N−H absorption occurs due to excess chain extender for which hydrogen-bond acceptors become increasingly scarce at chain extender stoichiometry above 100 mol %. This excess free N−H becomes important later in interpreting mechanical and structural measurements.

Figure 5 is a representative FTIR spectrum in the carbonyl region taken from the ϕ-gradient library at ϕ = 85 mol %, cured at 90 °C, along with the individually fitted peaks from the deconvolution procedure. The peaks in the spectrum are identified in Table 1. The

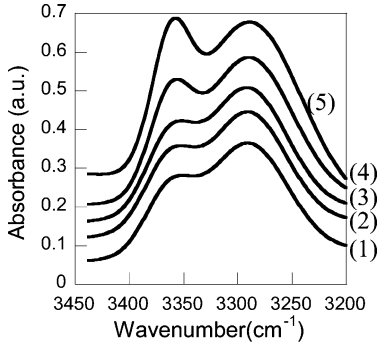

Figure 4. FT-IR spectra in the amine region for a composition-gradient poly(urethane−urea) library at different chain extender stoichiometric ratios; cured at 90 °C for 6 h. Bottom to top: (1) 85, (2) 100, (3) 116, (4) 132, and (5) 150 mol %. Spectra are arbitrarily offset.

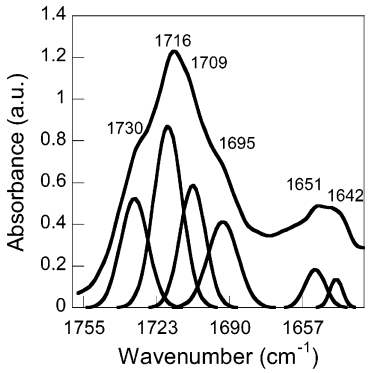

Figure 5. A representative spectrum in the carbonyl region for the composition-gradient poly(urethane−urea) library at chain extender composition of 85 mol % cured at 90 °C for 6 h.

Table 1. Absorption Band Assignments in the Carbonyl Region for Poly(urethane−urea)[15−17,23]

wavenumber (cm^{-1})	assignment
1730	free urethane carbonyl
1716	disordered, hydrogen-bonded urethane carbonyl
1709	ordered, hydrogen-bonded urethane carbonyl
1695	free urea carbonyl
1651	disordered, hydrogen-bonded urea carbonyl
1642	ordered, hydrogen-bonded urea carbonyl

urea peaks were used to estimate the urea−urea hydrogen bonding and the total urea hydrogen bonding using the approach developed by Ning et al.,[24] and the results are displayed in Figure 6.

Figure 6a shows the dependence of urea−urea hydrogen bonding on T and ϕ for the 25 library spectra and suggests that optimal mechanical strength will be observed in elastomers prepared at a $\phi = 85-116$ mol % stoichiometry and $T = 89$ °C. Figure 6b shows that the maximum total urea hydrogen bonding occurs at cure $T > 94$ °C. Although more total urea hydrogen bonds are formed at higher temperature, the important bidentate urea−urea hydrogen bonding responsible for hard-segment formation are maximized at $T = 89$ °C. In the previously published cure temperature study, we found that at $\phi = 95$ mol % optimum mechanical properties (elongation at break and impact strength) were observed at a cure temperature of 94 °C.[10] On the basis of these FTIR screens, the remainder of this report will focus on results obtained from characterizing ϕ-gradient libraries cured at 90 °C, since the primary focus of this paper is to understand the utilization of

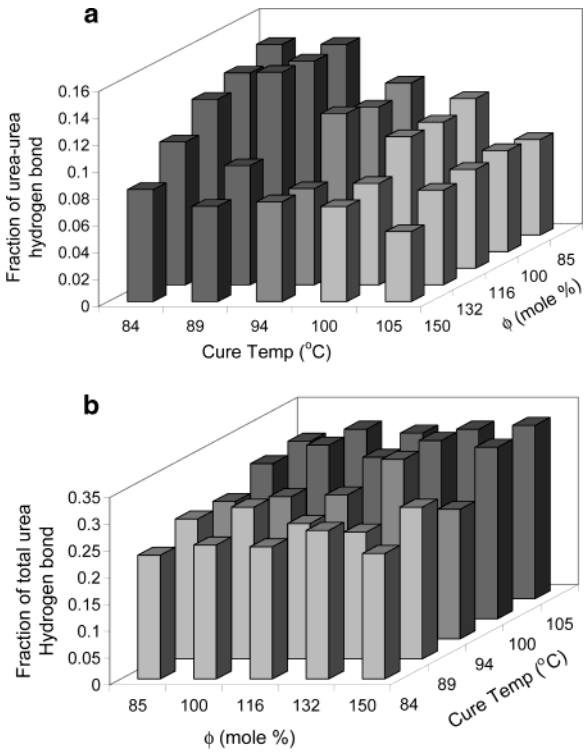

Figure 6. Dependence of urea hydrogen bonding on cure temperature and chain extender composition for poly(urethane−urea) library with orthogonal gradients in chain extender composition and cure temperature; cured for 6 h: (a) urea−urea hydrogen bonding, (b) total urea hydrogen bonding. Note: the axes in (a) and (b) are rotated to facilitate viewing of the trends.

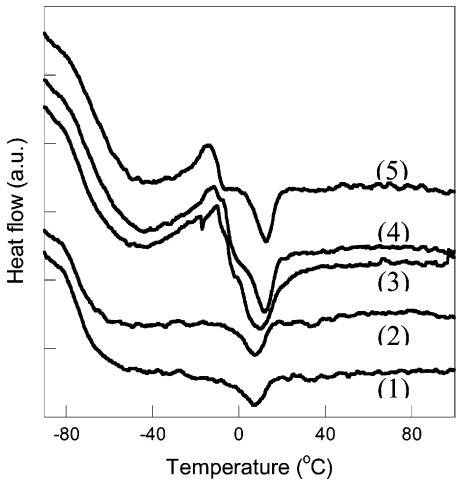

Figure 7. DSC curves (second heating) for uniform composition samples at different chain extender compositions; cured at 90 °C for 6 h. Bottom to top: (1) 85, (2) 100, (3) 116, (4) 132, and (5) 150 mol %. Curves are arbitrarily offset.

ϕ-gradient high-throughput characterization. No discernible difference was observed in the dependence of ϕ and cure T on the total urethane hydrogen bonding.

Glass transition temperature (T_g) is used often to indicate the degree of phase separation in polyurethanes and poly(urethane−urea)s. Figure 7 shows DSC traces (second heating run) of five poly(urethane−urea) samples, prepared at the same concentrations as those explored in the libraries. The soft segment T_g and other thermal characteristics are summarized in Table 2. DSC measurement for the pure soft-segment prepolymer (not included) showed a crystallization temperature at about

Table 2. DSC Data Obtained from Figure 8

chain extender composition (mol %)	$T_{crystallization}$ (°C)	$T_{melting}$ (°C)	soft segment T_g (°C)
85		8.4	−73.5
100		8.9	−72.4
116	−9.4	10.6	−70.9
132	−10.8	12.8	−67.1
150	−12.9	13.7	−65.7

−15 °C and a melting temperature of about 23 °C. The crystallization temperature (T_c) and melting temperature (T_m) are taken as the the maximum and minimum of the peaks, respectively. As shown in Table 2, there is an increase in soft segment T_g with an increase in chain extender composition. This increase in T_g suggests that phase mixing is enhanced when chain extender composition is increased, with more hard segments dissolving in the soft domains. Soft-segment crystallization exotherms were observed for samples with $\phi =$ 116, 132, and 150 mol %, with T_c decreasing with increasing ϕ as shown in Table 2, but crystallization exotherms were not observed at $\phi = 85$ and 100 mol %. At these two lower chain extender compositions, the hard domains form strong physical cross-links that probably hinder the molecular motion needed for strong soft-segment crystallization. T_m increases with an increase in ϕ (Table 2), which correlates with the decrease in T_c. This suggests that at higher ϕ, less energy is needed to orient the soft segments for crystallization because of reduced hard and soft domain network connectivity, resulting in purer crystals that melt at higher temperatures. These observations correlate with the reduced urea−urea hard-segment H-bonding as ϕ is increased and may lead to more thermoplastic or viscous behavior at high chain extender loadings.

Noncontact mode AFM has been used successfully to characterize the surfaces of a wide variety of phase-separated polymeric materials.[21,22,47−49] In noncontact AFM, different phases are detected by shifts in either the amplitude or phase of the oscillating tip due to van der Waals interactions between the cantilever tip and the sample.[47,48] For SPUUs with rigid hard domains and flexible soft domains, contrast between the two phases results from the differences in the local stiffness of the two domains. The high-modulus hard domains appear as light areas (+ phase shift), and the low-modulus soft segments appear as dark areas (− phase shift).[21,22,37,47−49] Figure 8 shows moderate force[48] AFM noncontact phase images taken at different positions on the surface of a SPUU ϕ-gradient library. The image at 85 mol % shows the highest cross-link density with hard domains (diameter ∼ 110−130 nm) evenly dispersed in the soft matrix. As the chain extender composition increases, the cross-link density decreases (fewer hard domains with larger interdomain spacing), and aggregation of hard domains is also observed. Reduced cross-link density and large hard domains tend to weaken the elastomeric (energy storage) capacity of the network and will eventually result in a loss of elastomeric character (thermoplastic or viscous behavior).

With the notable exception of the elastomer prepared at 85 mol %, all of the other compositions were completely dissolved in DMF after several hours. This suggests that the elastomers prepared at $\phi \geq 100$ mol % chain extender stoichiometry are void of chemical cross-links. These results are reasonable since cross-linking via biuret or allophanate formation is expected only when excess isocyanate is present, e.g., $\phi < 100\%$.

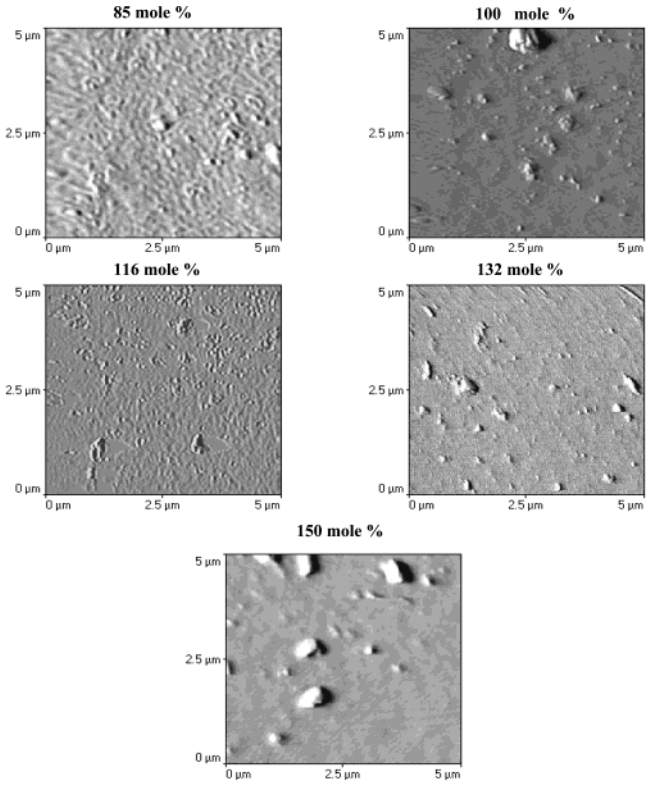

Figure 8. Noncontact mode AFM phase images at different chain extender compositions taken from a single composition-gradient poly(urethane−urea) library; cured at 90 °C for 6 h.

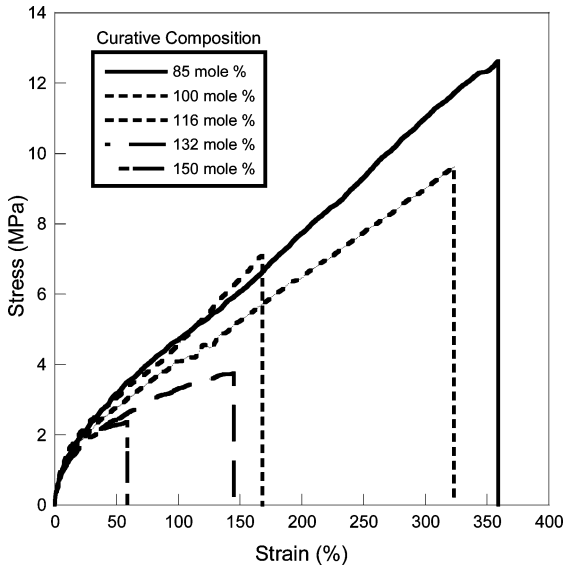

Figure 9. Stress−strain curves for a composition-gradient poly(urethane−urea) library at different chain extender stoichiometric ratios. Library was cured at 90 °C for 6 h; curves were obtained at an impact velocity of 0.89 m/s.

The chemically cross-linked 85 mol % elastomer was removed from the vial, carefully blotted to remove excess solvent, and weighed. The swell ratio (mass of swollen elastomer/initial mass of elastomer) was calculated to be 1.13. The magnitude of this ratio indicates that only a small fraction of hard domain is chemically cross-linked, and the majority of the hard domain results from physical cross-linking (hydrogen-bonding) between hard segments.

Figure 9 shows stress (σ) vs strain (ϵ) data from five different positions on a ϕ-gradient library at an impact-

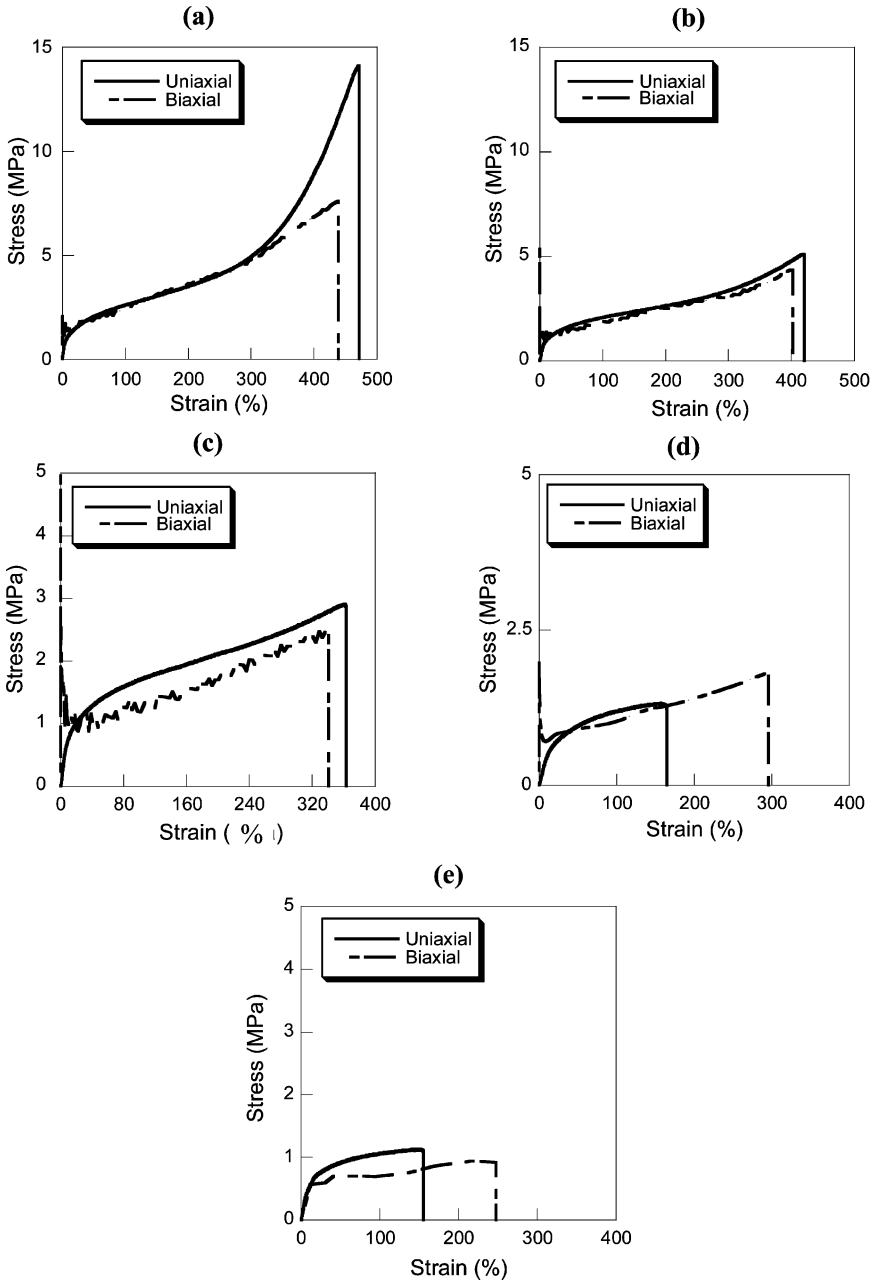

Figure 10. Stress−strain curves for uniform composition samples at different chain extender compositions; cured at 90 °C for 6 h. Curves were obtained from the HTMECH apparatus at $v_0 = 30$ mm/min and uniaxial loading using an Instron 5842 at $v_0 = 30$ mm/min: (a) 85, (b) 100, (c) 116, (d) 132, and (e) 150 mol %.

magnitude strain rate of $v_0 = 0.9$ m/s using the HT-MECH apparatus. Elongation at break, stress at break, and impact energy (area under curve) all decrease with increasing chain extender composition. The same trends were observed on multiple (3×) composition-gradient films and also from impacting uniform composition and cure *T* films. Figure 10 shows the σ vs ϵ curves obtained at a low strain rate of 30 mm/s using both the HTMECH apparatus and a commercial uniaxial tensile instrument (Instron). The stress plotted in Figure 9 is based on the raw force measurement that indicates only the *z*-component (vertical), whereas for comparison, the corrected in-plane radial stress is plotted in Figure 10. Similar trends are observed from both instruments: the elongation at break and the maximum stress at failure decrease with increasing chain extender composition, also observed in the high-velocity impact in Figure 9. Parts a and b of Figure 10 show the σ vs ϵ curves corresponding to 85 and 100 mol % chain extender, respectively, for both instruments. These two curves show three distinct regions characteristic of strain-crystallizing elastomers: an initial elastic rise, a plateau region, and a region with an upturn in slope due presumably to strain-induced crystallization.[43] These curves also show a nearly perfect overlay for both instruments between 50 and 300% strain. Also, the percent elongation for both instruments agrees very well within the errors of mechanical measurements.

The curves at 116, 132, and 150 mol % chain extender (Figure 10c−e) do not possess an upturn in slope after the plateau. Instead, the material fails within the plateau regime, suggesting that the excess chain extender causes a decrease in the capacity to store elastic energy. At higher chain extender composition, the material is probably acquiring plastic or viscoelastic character, as suggested by FTIR, DSC, and AFM data

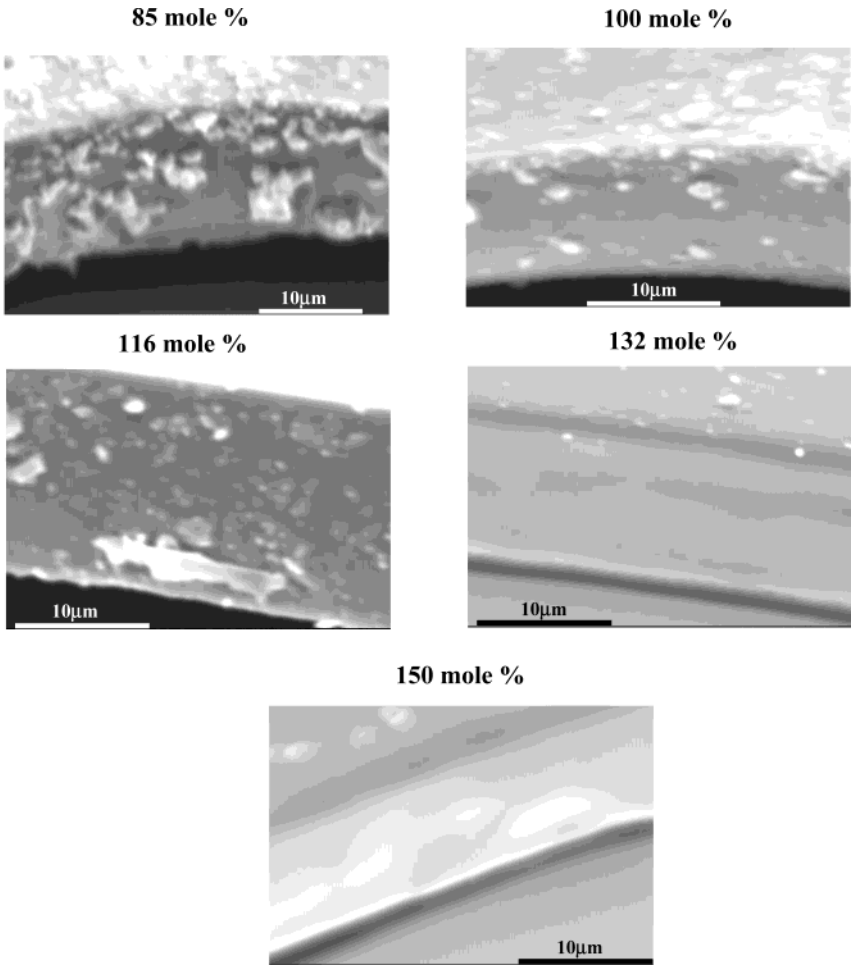

Figure 11. SEM images of the impact surfaces of the composition-gradient library film described in Figure 9.

presented above. As these energy release mechanisms increase, the stored stress will decrease, as indicated in both Figures 9 and 10 and captured with both radial and uniaxial approaches. Although the shapes are similar, the stress vs strain from HTMECH and conventional uniaxial do not agree quantitatively for the higher chain extender concentrations. In particular, at 132 and 150%, the percent elongation at break is significantly higher in the radial geometry. Previous experiments comparing equibiaxial to uniaxial deformation of elastomers have observed the same phenomena.[50] The radial geometry may permit more plastic deformation or viscous dissipation prior to failure and plans are underway to examine this hypothesis.

The mechanical trends observed in Figures 9 and 10 correspond well with the structural information obtained from AFM, DSC, and FTIR library screening. In addition, Figure 8 showed that the hard domain density decreases, and the interdomain spacing increases with increasing ϕ at a constant cure temperature of 90 °C. Figure 6 showed that bidentate urea−urea hydrogen-bonding diminished as ϕ and cure temperature increased. The excess H-bonded urea carbonyls are most likely H-bonding with urethane groups in the soft domains or urethanes that are mixed into the hard domains. These data, along with DSC measurements discussed above, indicate interdomain mixing and a structure that loses elastomeric character with increasing extender composition. At $\phi \geq 116\%$, chains may be "pulling out" of the network at sufficiently large deformations due to these network imperfections.

SEM images of the impacted surfaces were analyzed to gain an insight into the failure mechanisms at different chain extender compositions. Figure 11 shows that, in going from 85 to 150 mol % chain extender, a transition from a rough surface with many fragments to a smoother surface with few fragments occurs. This trend follows the general relationship between fracture surface roughness and tear strength of elastomers, where rougher surfaces have higher tear strengths.[51] At 132 and 150 mol %, the fractured surfaces were smooth, and the stress vs strain data (see Figures 9 and 10) showed no indication of the strain hardening typical of elastomers. With the structural data in Figures 6−8, these observations are strong evidence of a transition from purely elastomeric behavior toward a material with thermoplastic or viscous dissipation behavior.

Finally, we present a comparison of the "effective" secant modulus obtained from HTMECH with that obtained from a commercial uniaxial instrument (Instron 5842), shown in Figure 12. The secant modulus at 100% strain was calculated and compared for five different chain extender compositions, shown in Figure 10. A very good linear correlation was observed between the HTMECH (radial) and conventional (uniaxial) tensile measurements.

The radial secant modulus obtained from HTMECH differs by about 40% from the uniaxial modulus, but only at the highest moduli corresponding to the most highly elastic materials. The materials with high chain extender excess (lower modulus) show almost perfect agreement between the radial and uniaxial moduli,

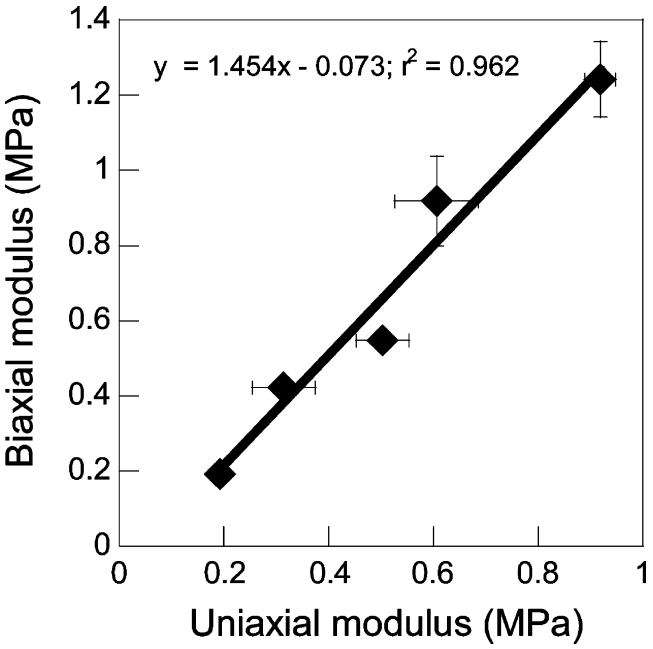

Figure 12. Comparison of the modulus at 100% strain using the stress−strain curves presented in Figure 10.

which may be due to a fortuitous cancellation in the nonlinear film profile errors (see Experimental Section). We tentatively attribute the differences in secant modulus for the nearly pure elastomeric materials (85 and 100% chain extender) to differences in the loading geometry that affect the onset and magnitude of both the nonlinear stress vs strain and nonaffine deformations. The nonlinear nature of stress developed in network deformation is known to depend on the loading geometry.[43] In addition, the onset of nonaffine deformation, thought to occur in the plateau region, allows molecular rearrangement of the network cross-links that reduce the total stored elastic energy.[43] In the uniaxial test two dimensions are free to adjust in response to the loading, whereas only one dimension is free of loading in the radial test.

Conclusions

The effect of chain extender composition on the mechanical properties of segmented poly(urethane−urea) was investigated using composition-gradient libraries coupled with a high-throughput mechanical characterization apparatus, HTMECH, developed recently by the authors. Stress−strain curves from the composition-gradient libraries showed an optimum in mechanical properties at the lowest chain extender composition examined, 85 mol %, which also agreed with measurements on uniform samples. At this stoichiometric ratio, the elastomer contained some chemical cross-linking, minimizing deformation of physically cross-linked hard domains and creating a stronger interfacial bond with the soft domain. Spectroscopic and microscopic measurements on the library suggest that at chain extender stoichiometry greater than 116 mol % excess hard segments are dispersed in the soft domain and urea−urea H-bonding is diminished, increasing the degree of phase mixing. Phase mixing tends to reduce the energy storage (elastomeric) character and can result in viscous or plastic energy dissipation processes. In this regard, rather simple FTIR screens of urea−urea hydrogen-bonding fractions are a reliable indicator of the trends observed in tensile strength and percent elongation. A comparison of the mechanical results obtained from HTMECH (radial) vs a commercial uniaxial instrument demonstrates a strong correlation between the secant modulus and trends in the tensile strength and percent elongation. These measurements serve to illustrate the utility of HTMECH as a convenient and accurate screening tool for mechanical properties in gradient polymer films.

Acknowledgment. The authors thank Air Products and Chemicals Inc. and Kimberly-Clark Corp. for providing materials and financial support. Joe-Lahai Sormana gratefully acknowledges 3M Corp. for supporting a GEM Fellowship.

References and Notes

(1) Meredith, J. C.; Karim, A.; Amis, E. J. *Macromolecules* **2000**, *33*, 5760.
(2) (a) Meredith, J. C.; Smith, A. P.; Karim, A.; Amis, E. J. *Macromolecules* **2000**, *33*, 9747. (b) Chattopadhyay, S.; Meredith, J. C. *Macromol. Chem. Phys.* **2004**, *25*, 275.
(3) Tomlinson, M. R.; Genzer, J. *Macromolecules* **2003**, *36*, 3449.
(4) Tomlinson, M. R.; Genzer, J. *Chem. Commun.* **2003**, 1350.
(5) Beers, K. L.; Douglas, J. F.; Amis, E. J.; Karim, A. *Langmuir* **2003**, *19*, 935.
(6) Ashley, K. M.; Meredith, J. C.; Amis, E. J.; Raghavan, D.; Karim, A. *Polymer* **2003**, *44*, 769.
(7) Smith, A. P.; Douglas, J. F.; Meredith, J. C.; Karim, A. *J. Polym. Sci., Part B: Polym. Phys.* **2001**, *39*, 2141.
(8) Meredith, J. C.; Sormana, J.-L.; Keselowsky, B.; Garcia, A. J.; Tona, A.; Karim, A.; Amis, E. J. *J. Biomed. Mater. Res.* **2003**, *66*, 483−490.
(9) Sormana, J.-L.; Meredith, J. C. *Mater. Res. Innov.* **2003**, *7*, 295.
(10) Sormana, J.-L.; Meredith, J. C. *Macromol. Rapid Commun.* **2003**, *24*, 118.
(11) Stafford, C. M.; Harrison, C.; Karim, A.; Amis, E. J. *Abstr. Pap. Am. Chem. Soc.* **2002**, *220-Poly Part 2*, 224.
(12) Hoogenboom, R.; Meier, M. A. R.; Schubert, U. S. *Macromol. Rapid Commun.* **2003**, *24*, 15.
(13) Chapon, P.; Mignaud, C.; Gilda, L.; Destarac, M. *Macromol. Rapid Commun.* **2003**, *24*, 87.
(14) Zhang, H.; Fijten, M. W. M.; Hoogenboom, R.; Reinierkens, R.; Schubert, U. S. *Macromol. Rapid Commun.* **2003**, *24*, 81.
(15) Paik Sung, C. S.; Hu, C. B.; Wu, C. S. *Macromolecules* **1980**, *13*, 111.
(16) Paik Sung, C. S.; Smith, T. W. *Macromolecules* **1980**, *13*, 117.
(17) Wang, C. B.; Cooper, S. L. *Macromolecules* **1983**, *16*, 775.
(18) Beck, R. A.; Truss, R. W. *Polymer* **1999**, *40*, 307.
(19) Wu, L.; You, B.; Li, D.; Qian, F. *J. Appl. Polym. Sci.* **2001**, *80*, 252.
(20) Wu, L.; You, B.; Li, D.; Qian, F. *Polym. Int.* **2000**, *49*, 1609.
(21) Garrett, J. T.; Runt, J. *Macromolecules* **2000**, *33*, 6353.
(22) Garrett, J. T.; Siedlecki, C. A.; Runt, J. *Macromolecules* **2001**, *34*, 7066.
(23) Ishihara, H.; Kimura, I.; Saito, K.; Ono, H. *J. Macromol. Sci., Phys.* **1974**, *B10*, 591.
(24) Ning, L.; De-Wing, W.; Sheng-Kang, Y. *Polymer* **1996**, *37*, 3577.
(25) Musselman, S. G.; Santosusso, T. M.; Barnes, J. D.; Sperling, L. H. *J. Polym. Sci., Part B: Polym. Phys.* **1999**, *37*, 2586.
(26) Osaki, K.; Kimura, S.; Nishizawa, K.; Kurata, M. *Macromolecules* **1980**, *14*, 456.
(27) Chiou, B.-S.; Schoen, P. E. *J. Appl. Polym. Sci.* **2002**, *83*, 212.
(28) Haska, S. B.; Bayramli, E.; Pekel, F.; Ozkar, S. *J. Appl. Polym. Sci.* **1997**, *64*, 2347.
(29) Spirkova, M.; Matejka, L.; Hlavata, D.; Meissner, B.; Pytela, J. *J. Appl. Polym. Sci.* **2000**, *77*, 381.
(30) Petrovic, Z. S.; Ilavsky, M.; Dusek, K.; Vidakovic, M..; Javni, I.; Banjanin, B. *J. Appl. Polym. Sci.* **1991**, *42*, 391.
(31) Petrovic, Z. S.; Javni, I.; Banhegyi, G. *J. Polym. Sci., Part B: Polym. Phys.* **1998**, *36*, 237.
(32) Petrovic, Z. S.; Ferguson, J. *Prog. Polym. Sci.* **1991**, *16*, 695.

(33) Spathis, G.; Niaounakis, M.; Kontou, E.; Apekis, L.; Pissis, P.; Christodoulides, C. *J. Appl. Polym. Sci.* **1994**, *54*, 831.
(34) Huang, J.; Zhang, L. *Polymer* **2002**, *43*, 2287.
(35) Huang, S.-L.; Lai, J.-Y. *Eur. Polym. J.* **1997**, *33*, 1563−1567.
(36) Petrovic, Z. S.; Javni, I.; Divjakovic, V. *J. Polym. Sci., Part B: Polym. Phys.* **1998**, *36*, 221.
(37) O'Sickey, M. J.; Lawrey, B. D.; Wilkes, G. L. *J. Appl. Polym. Sci.* **2002**, *84*, 229.
(38) Meredith, J. C.; Karim, A.; Amis, E. J. *MRS Bull.* **2002**, *27*, 330.
(39) Smith, A. P.; Douglas, J. F.; Meredith, J. C.; Amis, E. J.; Karim, A. *Phys. Rev. Lett.* **2001**, *87*, 15503.
(40) Green, A. E.; Adkins, J. E. *Large Elastic Deformations;* Oxford University Press: Oxford, 1960.
(41) Mooney, M. *J. Appl. Phys.* **1940**, *11*, 582.
(42) Yang, W. H.; Hsu, K. H. *J. Appl. Mech.* **1971**, *38*, 227.
(43) Wan, K.-T.; Liao, K. *Thin Solid Films* **1999**, *352*, 167.
(44) Liu, K. K.; Ju, B. F. *J. Phys. D: Appl. Phys.* **2001**, *15*, 91.
(45) Urayama, K.; Kawamura, T.; Kojiya, S. *Macromolecules* **2001**, *34*, 8261.
(46) Magnov, S. N.; Elings, V. *Polymer* **1997**, *38*, 297.
(47) McLean, R. S.; Sauer, B. B. *Macromolecules* **1997**, *30*, 8314.
(48) Grandy, D. B.; Hourston, D. J.; Price, D. M.; Reading, M.; Silva, G. G.; Song, M.; Sykes, P. *Macromolecules* **2000**, *33*, 9348.
(49) Dickie, R. A.; Smith, T. L. *J. Polym. Sci., Part A-2* **1969**, *7*, 687.
(50) Gent, A. N.; Pulford, C. T. R. *J. Mater. Sci.* **1984**, *19*, 3612.
(51) Kuriakose, B.; De, S. K. *J. Mater. Sci.* **1985**, *20*, 1864.

MA035385V